13. Kudoh, Y. & Kanzaki, M. *Int. Union of Crystallography, XVII Congress, Collected Abstr.* 317 (Int. Union Crystallography, Chester, UK, 1996).
14. Taylor, M. & Brown, G. E. *Am. Mineral.* **61,** 435–447 (1976).
15. Finger, L. W. & Hazen, R. M. *Acta Crystallogr. B* **47,** 561–580 (1991).
16. Brese, N. & O'Keefe, M. *Acta Crystallogr. B* **47,** 192–197 (1991).
17. Chuit, C., Corriu, R. J. P., Reye, C. & Young, J. C. *Chem. Rev.* **93,** 1371–1448 (1993).
18. Hemmati, M., Chizmeshya, A., Wolf, G. H., Poole, P. H., Shao, J. & Angell, C. A. *Phys. Rev. B* **51,** 14841–14848 (1995).
19. Wolf, G. H. & McMillan, P. F. *MSA Rev. Mineral.* **32,** 505–562 (1995).
20. Howells, E. R., Phillips, D. C. & Rogers, D. *Acta Crystallogr.* **3,** 210–214 (1950).
21. Wilson, A. J. C. *Acta Crystallogr.* **2,** 318–321 (1949).
22. Altomare, A. *et al. J. Appl. Crystallogr.* **27,** 435–436 (1994).
23. Finger, L. W. & Prince, E. *Natl Bur. Stand. Tech. Note* 854 (1974).
24. Robinson, K., Gibbs, G. V. & Ribbe, P. H. *Science* **172,** 567–570 (1971).

ACKNOWLEDGEMENTS. We thank R. Knoche, A. Sebald, R. Miletich, B. Poe for discussions and assistance. Experiments by N.L.R. in Bayreuth were performed under the EC 'Human Capital and Mobility' programme; T.F.F. was funded by an EC T.M.R. grant.

CORRESPONDENCE should be addressed to R.J.A. (e-mail: ross.angel@uni-bayreuth.de).

The effect of small-scale inhomogeneities on ozone depletion in the Arctic

S. Edouard*, B. Legras*, F. Lefèvre† & R. Eymard‡

* Laboratoire de Météorologie Dynamique du CNRS, Ecole Normale Supérieure, 24 Rue Lhomond, 75231 Paris Cedex 05, France
† CNRM, Météo-France/CNRS, 42 Avenue Coriolis, 31057 Toulouse Cedex, France
‡ Laboratoire Central des Ponts et Chaussées, 58 Boulevard Lefèvre, 75015 Paris, France

The chemical processes involved in the depletion of polar stratospheric ozone are now fairly well understood[1,2]. But the effect of small-scale stirring and mixing of the chemical species involved can be misrepresented in three-dimensional chemical-transport models because of their coarse resolution. Because of the non-linearities in the chemical rate laws, especially those involving chlorine in the main catalytic cycle, these effects can be important—particularly in the Arctic, where the polar vortex is less uniform and less isolated from surrounding air than in the Antarctic. Here we use a very-high-resolution model with simplified ozone-depletion chemistry to show that the depletion is sensitive to small-scale inhomogeneities in the distribution of reactant species. Under the conditions of the winter of 1994–95 the effect is large enough to account for the observed discrepancies of about 40% between modelled and observed ozone depletion in the Arctic environment[3–5].

In situ observations within the lower stratosphere show unambiguously the presence of sharp horizontal and vertical gradients, and of laminated structure, in the distribution of chemical components which are consistent with the current understanding of advection on isentropic surfaces[6]. Dynamically induced heterogeneities may persist for several weeks. Chemical reactions that depend on mixing of two components, or have nonlinear dependence on concentration, can be strongly affected[7]. State-of-the-art three-dimensional models of atmospheric chemistry can perform detailed modelling of the chemical reactions but are far from resolving the relevant transport and mixing processes[2]. We suggest here that taking into account small-scale inhomogeneities in the distribution of reactant species has a major effect on the predictions of such models.

Because stratospheric motion is thought to be constrained largely within horizontal layers down to scales of 1–10 km where three-dimensional motion is expected to dominate[8,9], we use here a two-dimensional horizontal transport model on the potential temperature surface $\theta = 450$ K with a simplified, albeit fairly realistic, model of the ozone chemistry. Very high resolution is obtained using a two-dimensional finite-volume scheme on the sphere[10] with 1,310,720 triangles and a mesh size $\delta h = 15$ km (δh being the distance between the centroids of two neighbouring triangles) which is corrected to ensure second-order accuracy, positivity and stability[11]. Because our aim is to estimate the order of magnitude of the effect of horizontal inhomogeneities, we neglect the vertical advection, which may alter the quantitative comparison with observations.

The ozone variation in the model is governed by the catalytic cycle known to be the most effective in the stratosphere[12], involving the self-reaction of ClO followed by the photolysis of its dimer Cl_2O_2 (refs 13, 14). Chlorine monoxide and its dimer

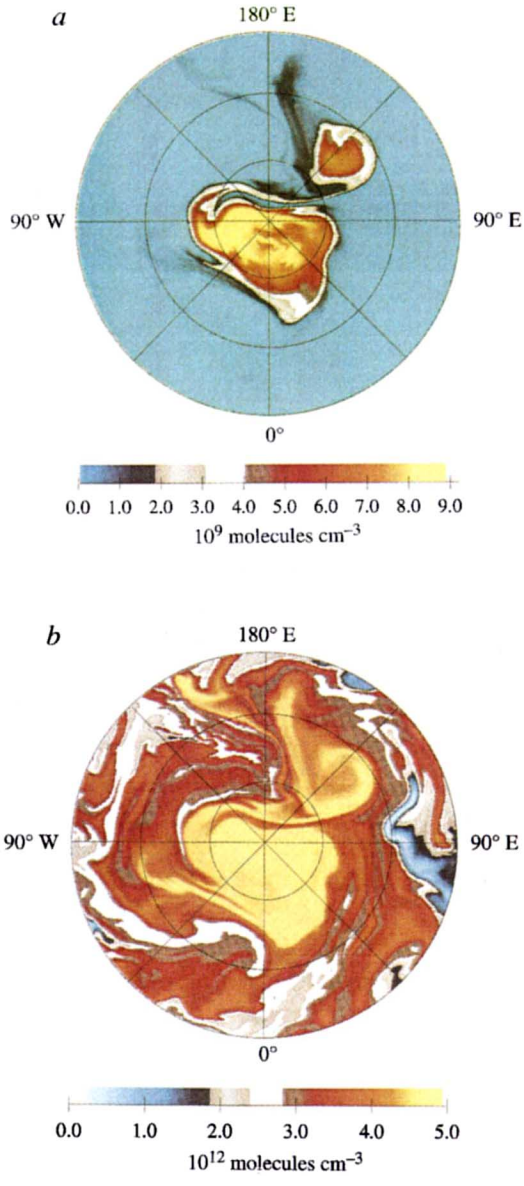

FIG. 1 *a*, Active chlorine concentration and *b*, ozone concentration at 12:00 GMT on 14 February at 450 K in the highest resolution (simulation E15). The projection is stereographic from 25° N to the pole. Latitude circles are at 45° and 70° N. The low level of ozone near 135° E, 60° N, over Siberia, cannot be due to mixing with subtropical air as ClO_x would also be diluted. This is a clear indication of depletion, also confirmed by ground-based measurements[21], which is due to the strong deformation of the vortex expelling activated polar air over mid-latitude regions where photolysis is intense.

are grouped under active chlorine ClO_x with $[ClO_x] = [ClO] + 2[Cl_2O_2]$. Ozone and ClO_x are the two chemical components transported by the flow. As the reactions following the photolysis of Cl_2O_2 are fast, the rate for the whole cycle during daytime is determined by the equilibrium between ClO and the dimer. Thereby, the ozone concentration evolves as:

$$\frac{d[O_3]}{dt} = -2k_{ClO+ClO}R[M][ClO]^2 \quad (1)$$

where the ambient concentration [M] depends on temperature and pressure, R is given by $R = J_{Cl_2O_2}/(J_{Cl_2O_2} + k_{Cl_2O_2}[M])$, $k_{ClO+ClO}$ is the reaction of the dimer formation and $k_{Cl_2O_2}$ is the reaction rate of its thermal decomposition[15]. The photodissociation frequencies $J_{Cl_2O_2}$ are interpolated from a pre-calculated table as a function of solar zenith angle. During daylight, [ClO] is inferred from $[ClO_x]$ using chlorine partitioning and the relation $(J_{Cl_2O_2} + k_{Cl_2O_2}[M])[Cl_2O_2] = k_{ClO+ClO}[M][ClO]^2$. Polar stratospheric clouds (PSC) are predicted as a function of temperature with no distinction between PSC I and type II water-ice PSCs, or inclusion of sedimentation processes. Rather, PSCs are assumed to form instantaneously at any grid point where $T < 195$ K. Active chlorine is released at the PSC's surface, at a constant rate $\alpha = 6 \times 10^4$ molecules cm^{-3} s^{-1}, and capped such that the total amount of ClO_x is less than 3 parts per billion by volume, p.p.b.v. Chlorine is deactivated through immediate recombination with NO_2 produced by photodissociation of HNO_3, setting a uniform and constant value of gaseous HNO_3 to 9 p.p.b.v. outside the PSC, reduced to 1 p.p.b.v. at the PSC's surface. Ozone loss is estimated by calculating the difference between the chemical mode (transport + chemistry) and the dynamical mode (transport only).

The data used are winds and temperatures analysed every 6 hours on 14 pressure levels, provided by the European Center for Medium-Range Weather Forecasts (ECMWF) in the horizontal resolution T42 (2.8° × 2.8°), and interpolated onto the $\theta = 450$ K isentropic surface[16]. Initial distribution of O_3 is taken from the three-dimensional transport-chemistry model REPROBUS[2] (2° × 2°), on 5 January 1995 at 12:00 GMT. The initial concentration of ClO_x is set to 2.62×10^9 molecules cm^{-3} (~1 p.p.b.v.). It is consistent to use fairly low-resolution wind as the strain is dominated by the largest eddies in layerwise flows[17]. More uncertainty remains on the possible role of small-scale temperature inhomogeneities in the generation of PSCs.

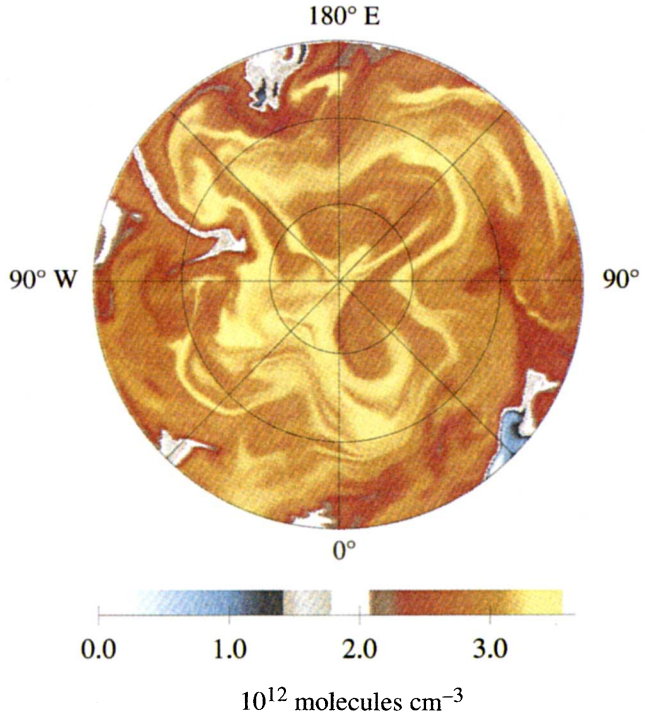

FIG. 2 Concentration of ozone at 12:00 GMT on 21 March at 450 K for the E15 simulation.

Temperatures in mid-December 1994 to mid-February 1995 were consistently cold, dropping continuously below the conventional threshold value for PSCs formation. By mid-January to mid-February, PSCs were located at the periphery of the polar vortex where strong winds moved substantial amounts of air mass through them, processing a large volume of air into chemically perturbed state. High local values of [ClO] build up in the model, up to 3.8×10^9 molecules cm^{-3} (~1.6 p.p.b.v.) on 23 January and 3.5×10^9 molecules cm^{-3} (~1 p.p.b.v.) consistent with observations[18], owing to the lack of PSCs and deactivation triggered by solar radiation. In early March, a cold spell again enhanced [ClO] to the level of early February, dramatically increasing ozone depletion during the month, as activated air was exposed to sunlight (Fig. 2). This tendency has been seen in satellite measurements[18]. At the end of March, the polar vortex was highly distorted by the final warming and strong stirring took place within the vortex but mostly at its periphery.

The sensitivity of ozone depletion to small-scale inhomogeneities in the distribution of reactant species arises from the non-linearity of the governing law (equation (1)). If ClO_x, initially released within a finite volume, is diluted by a factor of two, it contaminates a double volume but with half its initial concentration. Therefore, the total ozone destruction by the reaction of equation (1) is reduced by a factor of two with respect to the undiluted case. It is easy to see how crucial is the correct representation of dilution in modelling the ozone chemistry. Using the simulation performed at the highest available resolution $\delta h = 15$ km as a reference (simulation E15), we have investigated the effect of resolution by reducing δh to 30 km (simulation E30), and by further adding an explicit diffusion term with two different values for the diffusivity, $\nu_1 = 8 \times 10^4$ m^2 s^{-1} (simulation D1) and $\nu_2 = 3 \times 10^5$ m^2 s^{-1} (simulation D2) which provide effective horizontal resolution of ~100 and ~200 km (based on a strain value of 10^{-5} s^{-1}), within the range of the REPROBUS model.

The effect is indeed considerable (Fig. 3): maximum ozone depletion rises to 64.5% in E15 but drops to 53% in E30, and to 39.5% and 21.6% in D1 and D2. Main differences lie within the polar vortex where maintaining large values of $[ClO_x]$ over February and March enhances ozone depletion. Maximum depletion is located over filamentary structures inside the vortex, which replicate that of $[ClO_x]$, and are missed at lower resolution. The high-resolution calculation also predicts isolated ozone destruction of ~15% with peak values at 34.5% over the Eastern Pacific, near 30° N which is consistent with lidar observations reporting ozone depletion at middle latitudes[19]. This destruction can be traced back to the advection of a long and thin filament expelled from the polar vortex and carrying air rich in ClO_x towards middle latitudes where it reacts with O_3. This effect is weakened when the resolution is degraded and disappears in the most diffusive case (Fig. 3*b*–*d*).

The predicted averaged ozone loss within the vortex (Fig. 4*a*) ranges from 17% to 43% at the end of March. The comparison with SAOZ spectrometer measurements[22] measurements and the results of REPROBUS is made under the assumption that the variations in ozone column are mainly weighted by the contribution near 450 K. Our model clearly fails in reproducing the initial ozone loss in January. This discrepancy could be due to the absence of bromine which may account for 30–40% of the ozone loss in this period[20]. In addition, our model does not take into account the diabatic descent, nor the generation of ozone by photolysis of O_2, which may lower ozone loss in March[19]. Nevertheless, the main point arising from this comparison is that the discrepancy by a factor of 1.4 by the end of March between the data and the prediction of REPROBUS is very close to the predicted effect of resolution in our model. This result is not limited by the simplicity of our model and should apply under

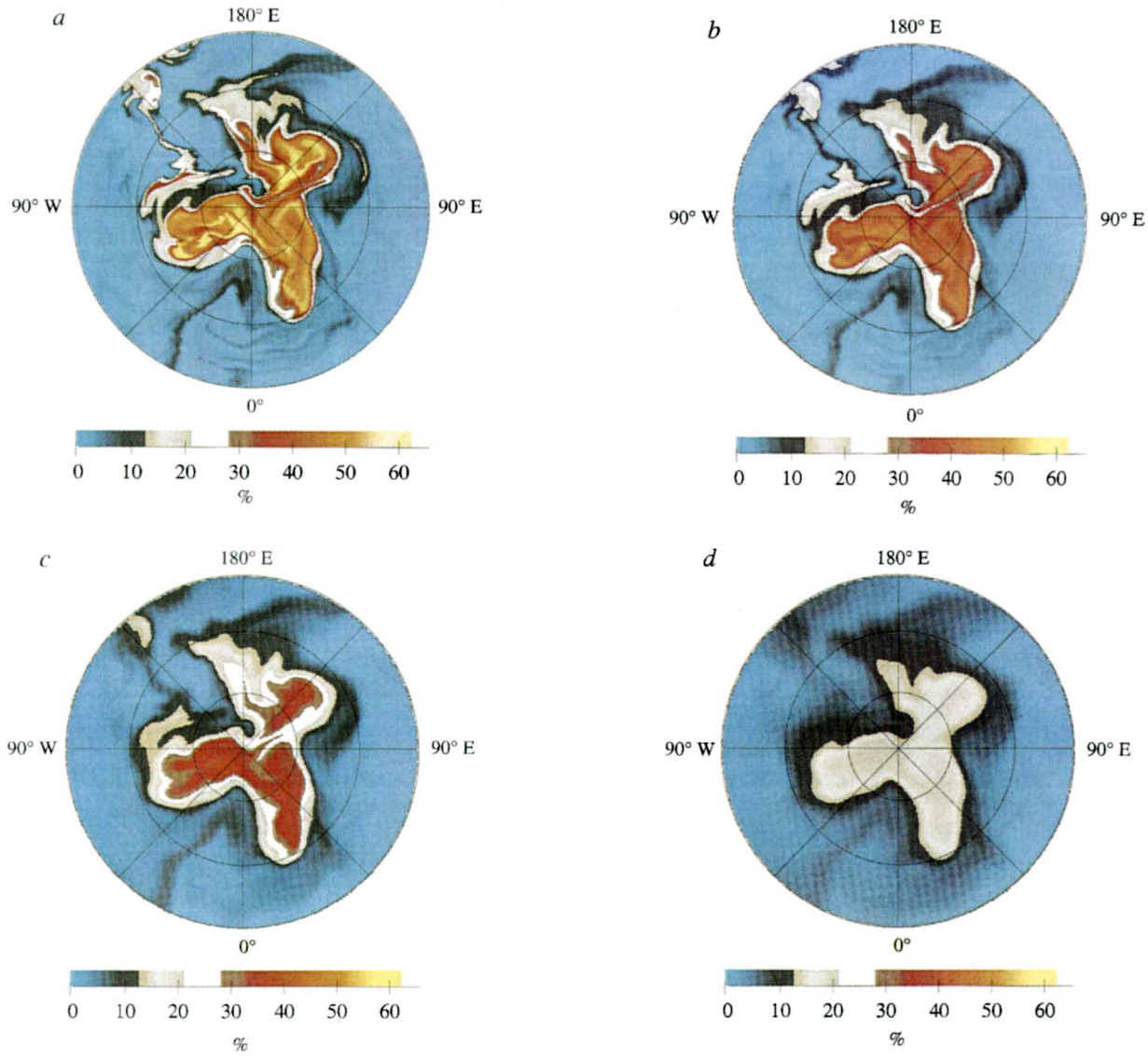

FIG. 3 Ozone loss (%) for the E15 simulation (*a*), the E30 simulation (*b*), the D1 simulation (*c*) and the D2 simulation (*d*), at 12:00 GMT on 30 March at 450 K.

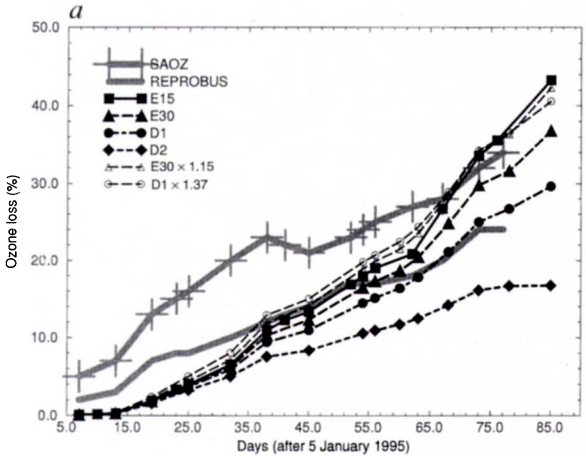

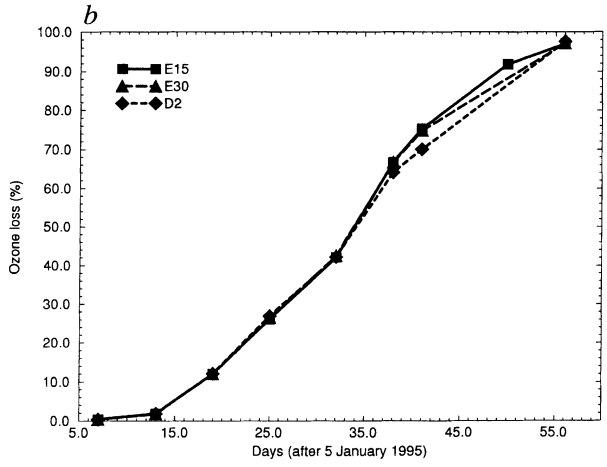

FIG. 4 *a*, Ozone loss (%) within the vortex as a function of time, at 450 K, from 5 January to 30 March, for the E15 simulation (solid line, squares), the E30 simulation (long dashed line, triangles), the D1 simulation (dot-dashed line, circles) and the D2 simulation (dashed line, diamonds). SAOZ measurements (grey line, crosses) and REPROBUS results (grey line, no plotting symbols) are adapted from refs 3 and 4. *b*, Ozone loss (%) within the vortex as a function of time under Antarctic conditions (increased α), from 5 January to 1 March, for the E15 simulation (solid line, squares), the E30 simulation (long dashed line, triangles) and the D2 simulation (dashed line, diamonds). The boundary of the polar vortex at 450 K is defined by the contour where potential vorticity is 25×10^{-6} K m^2 kg^{-1} s^{-1}.

more realistic conditions as long as ozone depletion by chlorine dominates in the Arctic.

It is important to note that ozone is only partially destroyed. In the Antarctic, where denitrification makes available a large amount of chlorine, almost complete destruction of ozone is observed. One would expect that the dilution effect here may not be as important as in the Arctic. We tested this by artificially increasing α by a factor of 10 in our calculation to imitate the conditions prevailing in the Antarctic. Much higher depletion is then observed (Fig. 4*b*) but there is almost no sensitivity to dilution. This is not to say that mixing effects are absent. The relevant mechanism, not considered here, is the sensitivity of chlorine deactivation to the mixing of denitrified polar air with subtropical air[8] for which higher diffusivity or the lack of numerical resolution enhances the chemical reactivity.

We investigated whether the effect of small-scale inhomogeneities could be parametrized in low-resolution three-dimensional chemical models. A good fit to the curve of total ozone depletion for simulation E15 can be obtained by multiplying the corresponding curves for E30 and D1 respectively by a factor of 1.15 and by a factor of 1.37 (dashed curve with empty symbols in Fig. 4*a*) which is equivalent to increasing $k_{ClO+ClO}$ in equation (1). In the case of chlorine deactivation, where chemical compounds are initially separated, Thuburn and Tan[8] propose decreasing the reaction rate in the model. The influence of dynamics on chemistry is complex so that designing robust parametrizations of small-scale inhomogeneities might not prove an easy task. Meanwhile modellers should be aware that their results depend on the spatial resolution and that ultra-high-resolution modelling might be necessary to reach accurate results. □

Received 7 June; accepted 14 October 1996.

1. Webster, C. *et al. Science* **261,** 1130–1133 (1993).
2. Lefèvre, F. *et al. J. Geophys. Res.* **99,** 8183–8195 (1994).
3. Goutail, F. *et al.* in *Air Pollution Res. Rep.* No. 56 (eds Pyle, J. A., Harris, N. R. P. & Amanatadis, G. T.) 574–579 (European Communities, Brussels, 1996).
4. Goutail, F. *et al. J. Atmos. Chem.* (submitted).
5. Chipperfield, M. *et al. J. Atmos. Chem.* (submitted).
6. Holton, J. R. *et al. Rev. Geophys.* **33,** 403–436 (1995).
7. Edouard, S., Legras, B. & Zeitlin, V. *J. Geophys. Res.* **101,** 16771–16779 (1996).
8. Thuburn, J. & Tan, D. *J. Geophys. Res.* (submitted).
9. Haynes, P. H. & Anglade, J. *J. Atmos. Sci.* (in the press).
10. Selmin, V. *Comput. Meth. Appl. Mech. Eng.* **102,** 107–138 (1993).
11. van Leer, B. *J. Comput. Phys.* **23,** 276–299 (1977).
12. Salawitch, R., Wofsy, S. & Gottlieb, E. P. *Science* **261,** 1146–1149 (1993).
13. Molina, M. J. & Molina, L. T. *J. Phys. Chem.* **91,** 433–436 (1987).
14. Molina, M. J., Tso, T., Molina, L. T. & Wang, F. *Science* **238,** 1253–1257 (1987).
15. DeMore, W. B. *NASA Tech. Rep. 92–20* (Jet Propulsion Lab., Pasadena, 1992).
16. Brunet, G., Vautard, R., Legras, B. & Edouard, S. *Mon. Weath. Rev.* **123,** 1037–1058 (1995).
17. Haynes, P. H. & Ward, W. E. *J. Atmos. Sci.* **50,** 3431–3453 (1993).
18. Manney, G. *et al. Geophys. Res. Lett.* **23,** 85–88 (1996).
19. Donovan, D. *et al. Geophys. Res. Lett.* **22,** 3489–3492 (1996).
20. Chipperfield, M., Cariolle, D. & Simon, P. *Geophys. Res. Lett.* **21,** 1467–1470 (1994).
21. Bojkov, R. *et al. Geophys. Res. Lett.* **22,** 2729–2732 (1995).
22. Pommereau, J. P. & Goutail, F. *Geophys. Res. Lett.* **15,** 891–893 (1988).

ACKNOWLEDGEMENTS. We thank P. Haynes for comments. Computations were performed using the resources provided by IBM at Institut Pierre-Simon Laplace and by Institut du Développement et des Ressources en Informatique Scientifique (IDRIS).

Possible role of dust-induced regional warming in abrupt climate change during the last glacial period

Jonathan Overpeck*†, David Rind‡, Andrew Lacis‡ & Richard Healy§

* NOAA Paleoclimatology Program, National Geophysical Data Center, 325 Broadway, E/GC, Boulder, Colorado 80303, USA
† Institute of Arctic and Alpine Research and Department of Geological Sciences, University of Colorado, Boulder, Colorado 8039, USA
‡ NASA Goddard Institute for Space Studies, 2880 Broadway, New York, New York 10025, USA
§ Center for Climate Systems Research, Columbia University, New York, New York 10027, USA

Records from loess, sediments and ice cores indicate that the concentrations of tropospheric aerosols were higher in glacial periods than they are today, and that they peaked just before glacial terminations[1–10]. Energy-balance models have suggested[11–14] that these high glacial aerosol loadings were a source of glacial cooling of the order of 1–3 °C. Here we present a different view based on three-dimensional climate simulations, which suggest that high glacial dust loading may have caused significant, episodic regional warming of over 5 °C downwind of major Asian and ice-margin dust sources. Less warming was likely close to and over the oceans because of local cooling by sea-salt and marine sulphate aerosols. Abrupt changes in dust loading are associated with the Dansgaard–Oeschger and Heinrich climate events and with glacial termination[3,8,15], suggesting that dust-induced warming may have played a role in triggering these large shifts in Pleistocene climate.

To examine the potential role of tropospheric dust in glacial climates, we carried out two sets of simulations with the NASA Goddard Institute for Space Studies (GISS) general circulation model (Model II, using 4° × 5° latitude–longitude resolution, full seasonal cycle, interactive land surface and clouds[16,17]). First, two five-year simulations (with fixed sea surface temperature, SST) were run with identical late glacial conditions[18] but with different atmospheric dust loadings. In the 'modern-dust' simulation, we used present-day monthly mean dust[19] as shown in Fig. 1*a*, *b*). In the 'glacial-dust' simulation, average modern-day desert silt and clay mineral dust[19,20] was prescribed with peak abundance in the lower troposphere over each 4° × 5° model grid box containing some fraction of the North American ice sheet or desert (Fig. 1*c*). The optical depth of glacial dust was specified to be 0.168, in accordance with ice-core observations[1,7], distributed uniformly over the affected gird boxes.

Comparing 'glacial-dust' with 'modern-dust' simulations shows warming patterns (Fig. 2*a*) that differ substantially from the pattern of applied radiative forcing (Fig. 1*c*); this points to the importance of regional differences in feedback interactions that arise from changes in static stability due to solar heating and longwave heating/cooling by dust aerosols[19,20]. This behaviour differs from the classical response inferred from changes in energy balance arising from aerosol effects on planetary albedo[21,22]. Except for regions of northern Canada and Alaska, the dust-induced average annual warming was greater at progressively higher latitudes, and was greatest (up to 4.4 °C) in regions with dust over high-albedo snow- and ice-covered areas. Because the SSTs were fixed in these simulations, the global temperature change was small. Contributing changes in cloud cover, atmospheric water vapour, and surface albedo are listed in Table 1.

Our results are consistent with recent assessments of how mineral dust affects present climate[19,20]. Decreased backscattering of incident solar radiation occurs when the aerosol overlies high-albedo snow- or ice-covered surfaces, whereas solar backscattering is increased when the dust overlies dark land and ocean surfaces. The effective cloud single scattering albedo decreases when dust occurs within clouds[19]. In addition to its shortwave effect, dust loading also contributes a small, but significant, amount of greenhouse warming through increased absorption of thermal radiation[17]. Within this general context, specific causes of surface warming varied from region to region. Typically, regions with reduced planetary albedo are associated with increased solar